Electronic Supporting Information

A novel approach to describe the electric double layer structure of water-in-salt electrolytes in porous carbon electrodes

M. Tauhidul Islam[1], Harald Fitzek[2,3], Bernhard Gollas[1], Qamar Abbas[1,4*]

[1]*Institute for Chemistry and Technology of Materials, Graz University of Technology, Stremayrgasse 9, 8010 Graz, Austria.*
[2]*Graz Centre for Electron Microscopy, Steyrergasse 17, 8010 Graz, Austria.*
[3]*Institute of Electron Microscopy and Nanoanalysis, Graz University of Technology, Steyrergasse 17, 8010, Graz, Austria.*
[4]*Institute of Chemistry and Technical Electrochemistry, Poznan University of Technology, Berdychowo 4, 60965 Poznan, Poland.*

[*]Corresponding author email: qamar.abbas@tugraz.at

Table of contents

***Method S1*:** Electrochemical impedance spectroscopy (EIS) of non-porous electrodes

A two-electrode Swagelok cell with a cylindrical PTFE (polytetrafluoroethylene) spacer ring positioned between two stainless-steel rod current collectors (12.7 mm diameter) (**Figure S1a**) was used for measuring the electrolyte resistance. For each measurement, the same volume of electrolyte solution was placed into the spacer ring, which had a thickness of 2 mm and a diameter of 8 mm. Electrochemical impedance spectra were recorded over the frequency range of 100 kHz to 1 mHz with a single sine sinusoidal signal at open circuit voltage (≈30 mV) using a BioLogic VMP-300 Potentiostat (France).

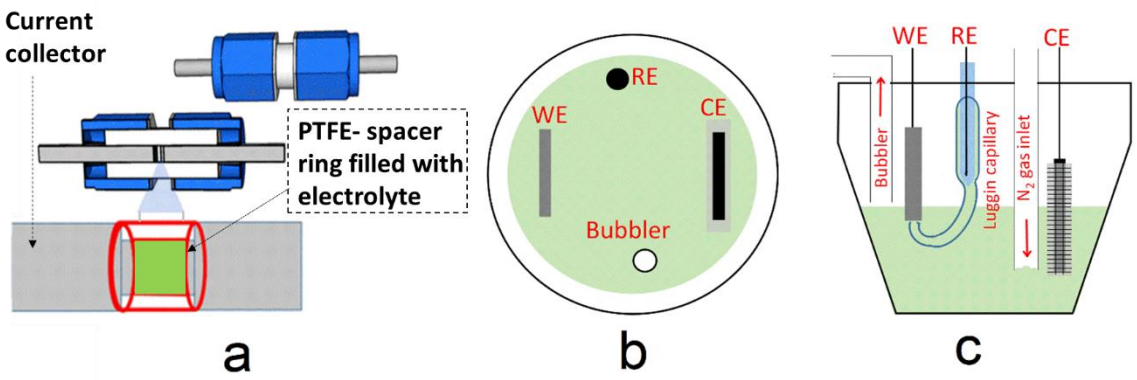

Figure S1: Schematic diagram of the cell utilized for **(a)** Schematic diagram of the Swagelok cell utilized for potentiostatic electrochemical impedance spectroscopy of non-porous electrodes at open circuit potential (≈ 30 mV) at a room temperature of 25 ℃; **(b)** top and; **(c)** side view of the three-electrode electrochemical glass cell setup used in this work for recording cyclic voltammograms of a non-porous glassy carbon electrode.

Method S2: Cyclic voltammetry of non-porous glassy carbon electrode in electrochemical glass cell

Cyclic voltammograms (CVs) were recorded with a scan rate of 10 $mV \cdot s^{-1}$ using a Metrohm Autolab PGSTAT128N (Netherlands) at room temperature (25 ℃). An electrochemical glass cell with a three-electrode configuration was utilized for cyclic voltammetry as shown in **Figures S1b** and **S1c**. A saturated calomel electrode (SCE) ($Hg/HgCl_2$ in 3.5 M KCl, 0.241 V vs. SCE) was fitted into a Luggin capillary and served as reference electrode. The tip of the Luggin capillary was adjusted at a distance of 1 mm from the Metrohm 6.1241.060 glassy carbon working electrode with a geometric surface area of 0.071 cm^2. A rectangular 2×1 cm^2 Pt-mesh having a wire diameter of 0.1 mm was used as the counter electrode. Before each electrochemical measurement, the electrolyte solution was de-aerated with N_2 gas for 120 min. Then the bubbling was interrupted maintaining a continuous N_2 flow over the solution. Before each measurement, the working electrode was carefully polished on a polishing cloth with Al_2O_3 powder (0.3 µm grain size)-DI H_2O slurry and thoroughly rinsed in DI water. The glass cell setup was placed inside a Faraday cage for avoiding any unwanted external electric field disturbance and the grounding cable of the Autolab was connected to the Faraday cage.

Method S3: Electrochemical capacitor cell assembly and characterization[1]

Activated porous carbon sheets served as electrodes in capacitor cells. These sheets were prepared from a blend of 90 wt.% YP80 F commercial battery carbon (Kuraray, Japan), 5 wt.% carbon black SUPER C65 (Imerys) as a conductive additive, and 5 wt.% polytetrafluoroethylene (60 wt.% suspension in water, Sigma-Aldrich) as a binder. The components were mixed in isopropanol at a wt. ratio of 1:20 (material to solvent). This mixture was stirred at 70 °C until a uniform dough had formed, which was then rolled onto a glass plate with a SS rod to create a ≈140 μm thick sheet. The carbon sheet was dried overnight at 80 °C. Two 1.0 cm diameter electrode disks, cut from the prepared carbon sheet, were used as positive and negative electrodes (stainless steel rod with 12.7 mm diameter) in the two-electrode symmetric Swagelok-type capacitor cells, sandwiching a 1.2 cm diameter glass microfiber separator (Whatman GF/A, ≈260 μm thick). Electrochemical impedance spectra (EIS) were recorded over a frequency range from 1 MHz to 1 mHz using a single sinusoidal signal at open circuit potential of ≈30 mV, with each data point representing the average of five measurements at each frequency. The electrochemical impedance spectra of capacitor cells were recorded at 0.4, 0.8, and 1.2 V to estimate the energy density. Capacitance, power, and energy values were normalized to account for the 90 wt.% YP80 F, based on the total mass of both electrodes.

Method S4: Determination of different electrochemical quantities of non-porous electrodes in water-in-LiTFSI electrolyte using EIS.[2]

Angular frequency: $\omega = 2 \cdot \pi \cdot f$ ***(S1)***

Real part of the permittivity: $\varepsilon' = \frac{d}{A \cdot \omega \cdot \varepsilon_0} \cdot \frac{Z''}{Z'^2 + Z''^2}$ ***(S2)***

Imaginary part of the permittivity: $\varepsilon'' = \frac{d}{A \cdot \omega \cdot \varepsilon_0} \cdot \frac{Z'}{Z'^2 + Z''^2}$ ***(S3)***

Capacitance of ideal capacitor in vacuum: $C_0 = \frac{A \cdot \varepsilon_0}{d}$ ***(S4)***

Real part of capacitance: $C' = \varepsilon' \cdot C_0$ ***(S5)***

Imaginary of capacitance: $C'' = \varepsilon'' \cdot C_0$ ***(S6)***

Dielectric loss: $tan\ \delta = \frac{\varepsilon''}{\varepsilon'}$ ***(S7)***

Real part of admittance or conductance: $Y' = \frac{\varepsilon'' \cdot \omega \cdot A \cdot \varepsilon_\circ}{d}$ ***(S8)***

Imaginary part of admittance or susceptance: $Y'' = \frac{\epsilon' \cdot \omega \cdot A \cdot \varepsilon_\circ}{d}$ ***(S9)***

Real part of conductivity: $\sigma' = \frac{Y' \cdot d}{A}$ ***(S10)***

Imaginary part of conductivity: $\sigma'' = \frac{Y'' \cdot d}{A}$ ***(S11)***

Here, f is the frequency, A is the geometric area of the electrode; d is the distance between electrodes; Z' is the real component of the impedance; Z'' is the imaginary component of the impedance, and ε_0 is the vacuum permittivity.

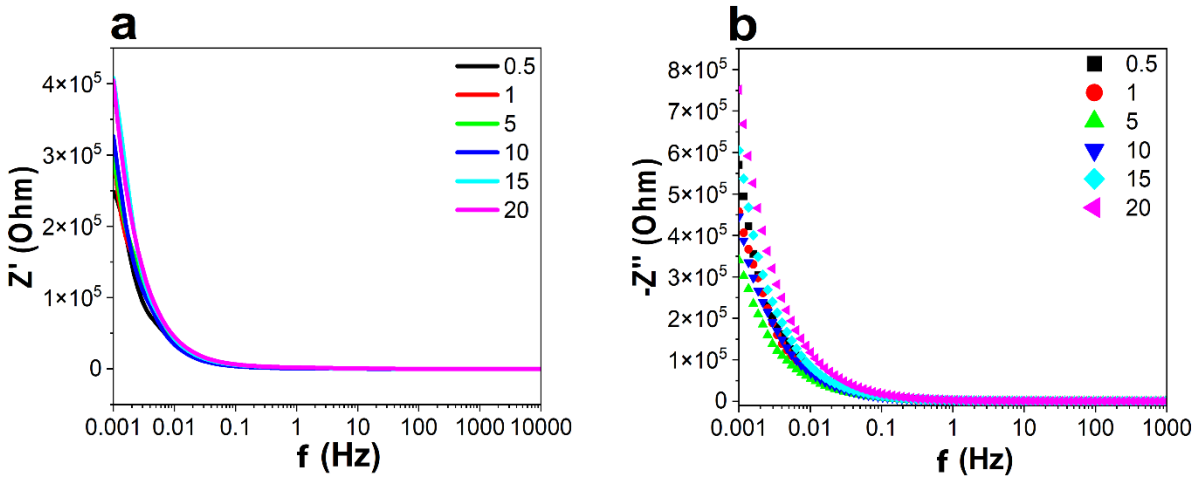

Figure S2: Effect of LiTFSI concentration on the **(a)** real and **(b)** imaginary part of the impedance vs frequency measured with a non-porous stainless-steel electrode

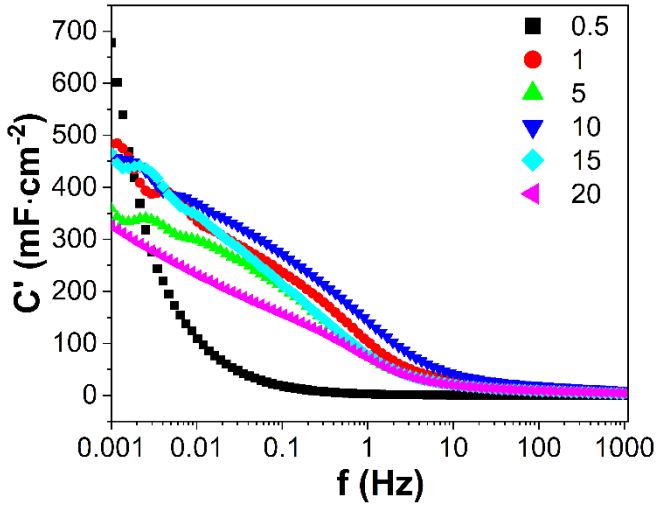

Figure S3: Effect of LiTFSI concentration on the real part of the capacitance vs frequency measured with a non-porous stainless-steel electrode

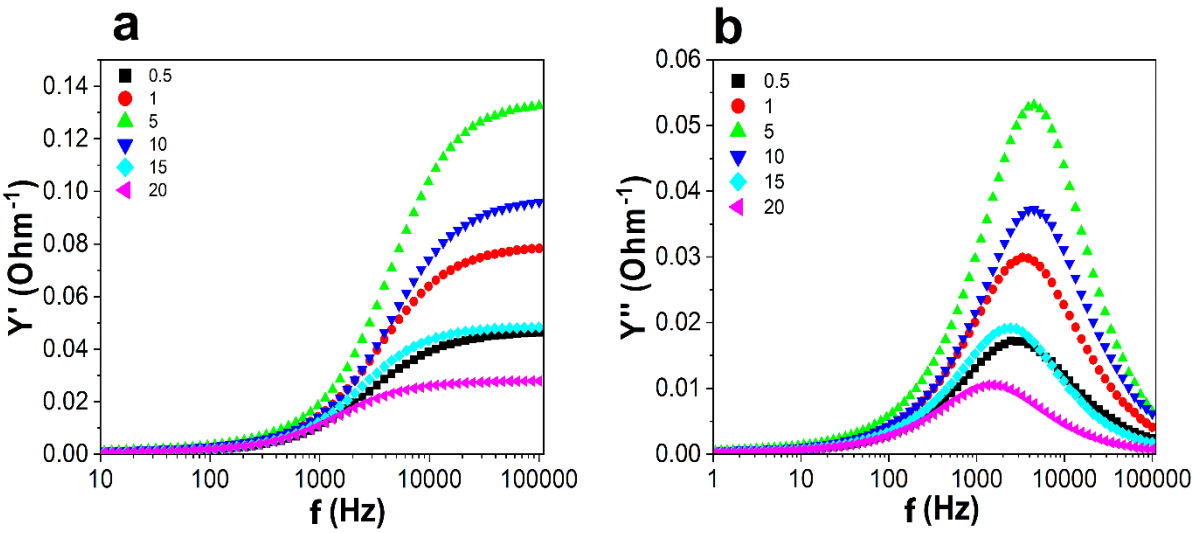

Figure S4: Effect of LiTFSI concentration on the **(a)** real and **(b)** imaginary part of the admittance vs frequency measured with a non-porous stainless-steel electrode

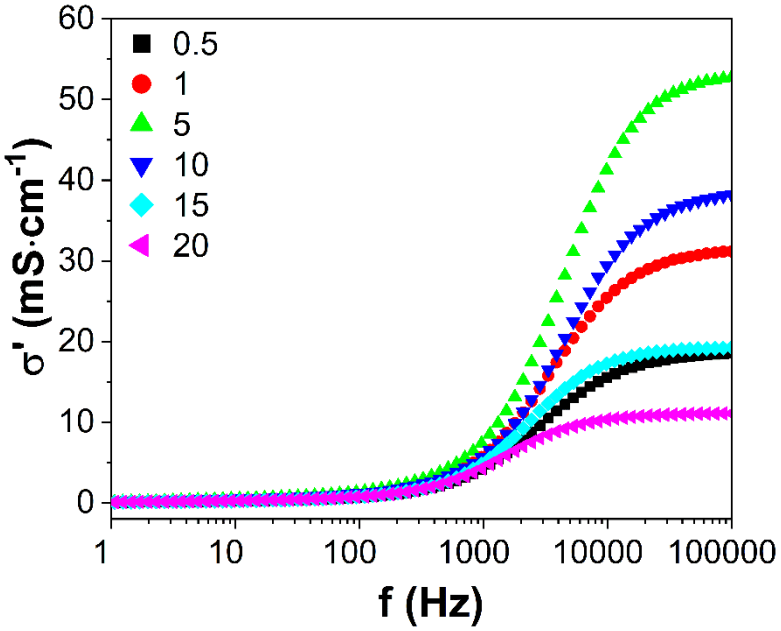

Figure S5: Effect of LiTFSI concentration on the on the real part of the ionic conductivity vs frequency measured with a non-porous stainless-steel electrode

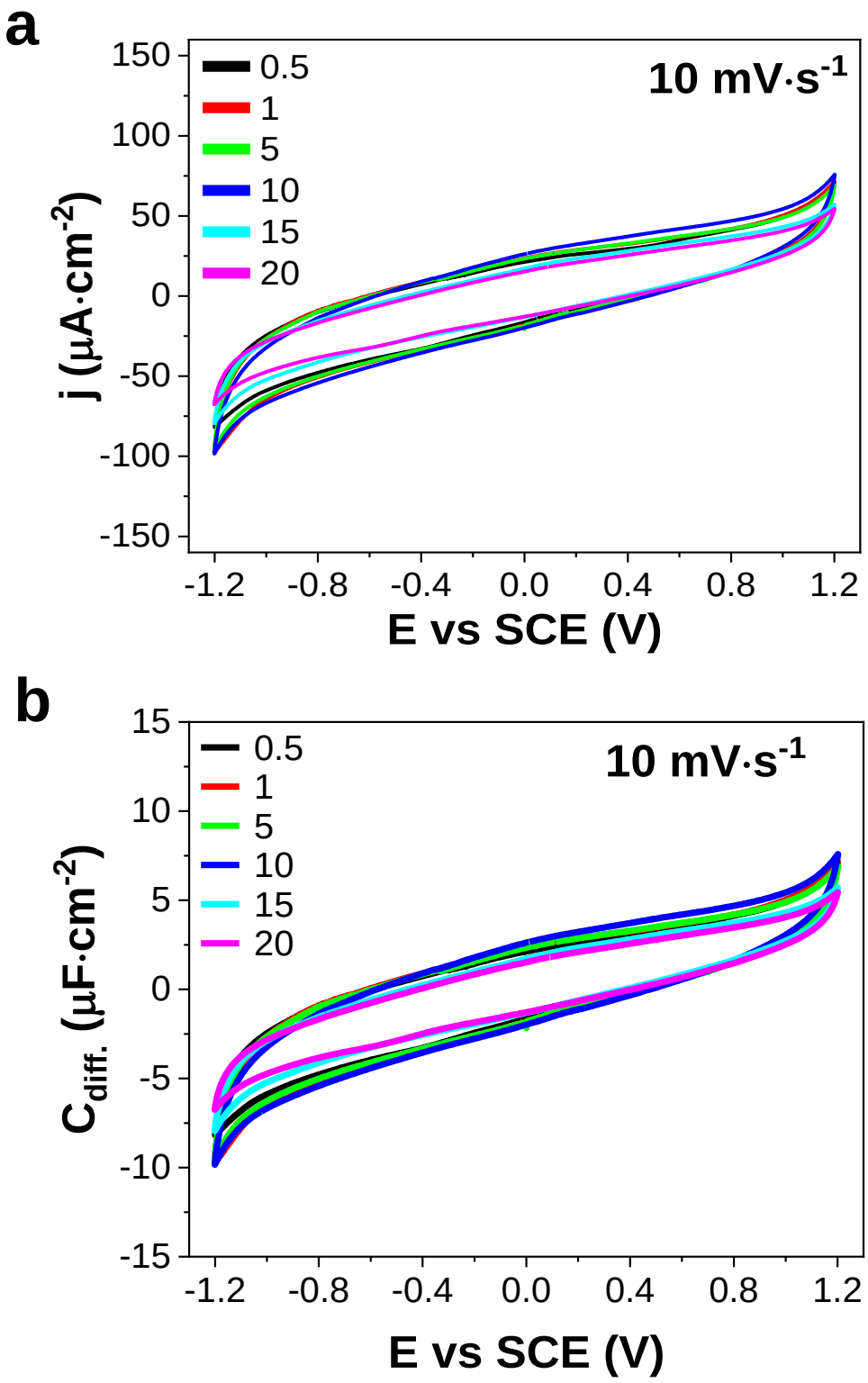

***Figure S6*:** Cyclic voltammograms measured with a non-porous glassy carbon electrode in different LiTFSI solutions using a three-electrode glass cell at 25 ℃ and a scan rate of 10 $mV \cdot s^{-1}$. **a)** Current density and **b)** differential capacitance as a function of applied potential versus saturated calomel electrode.

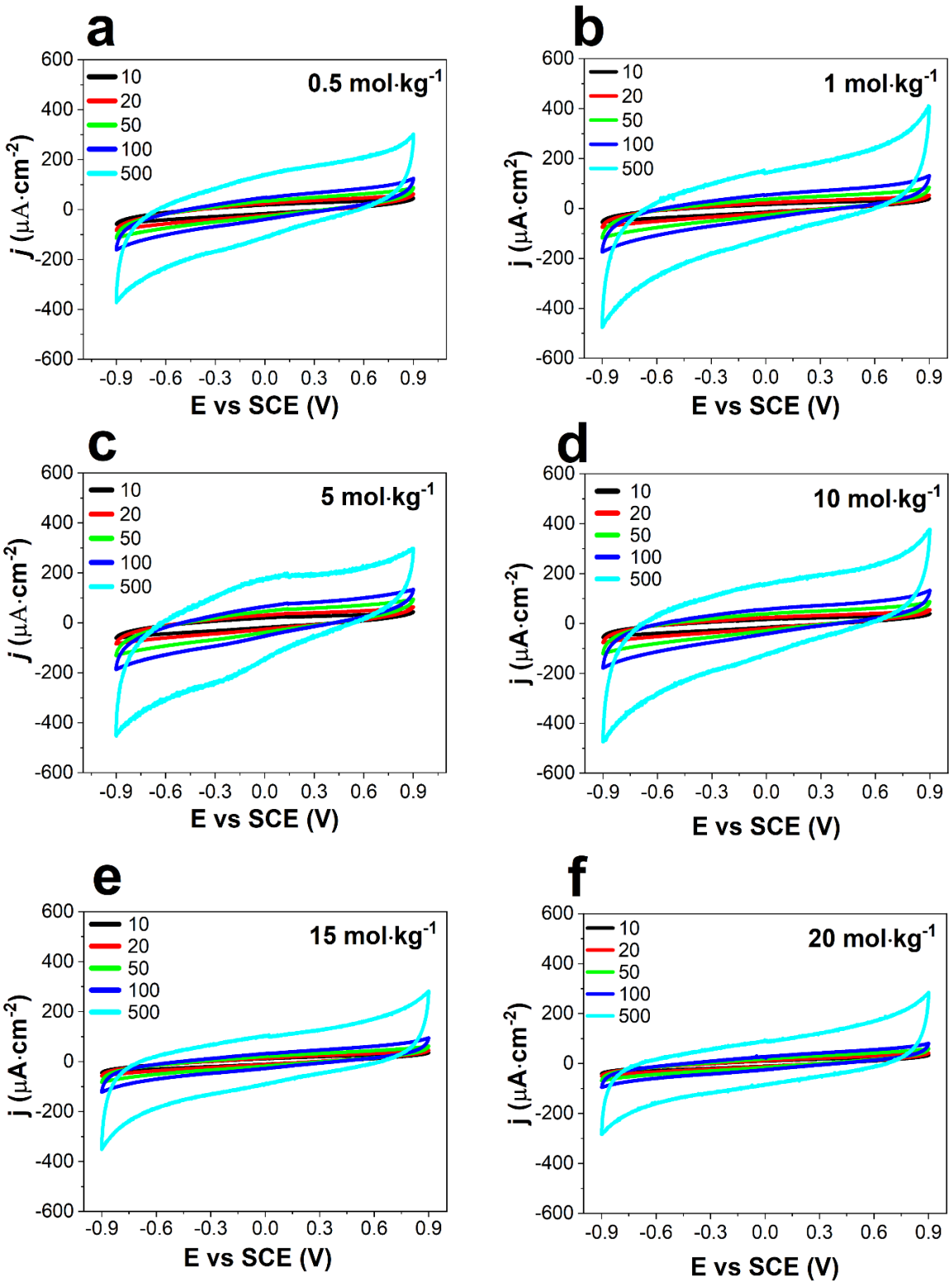

***Figure S7*:** Cyclic voltammograms measured with a non-porous glassy carbon electrode in different LiTFSI solutions (**a-f**) using a three-electrode glass cell at 25 ℃ and scan rates of 10, 20, 50, 100 and 500 $mV \cdot s^{-1}$.

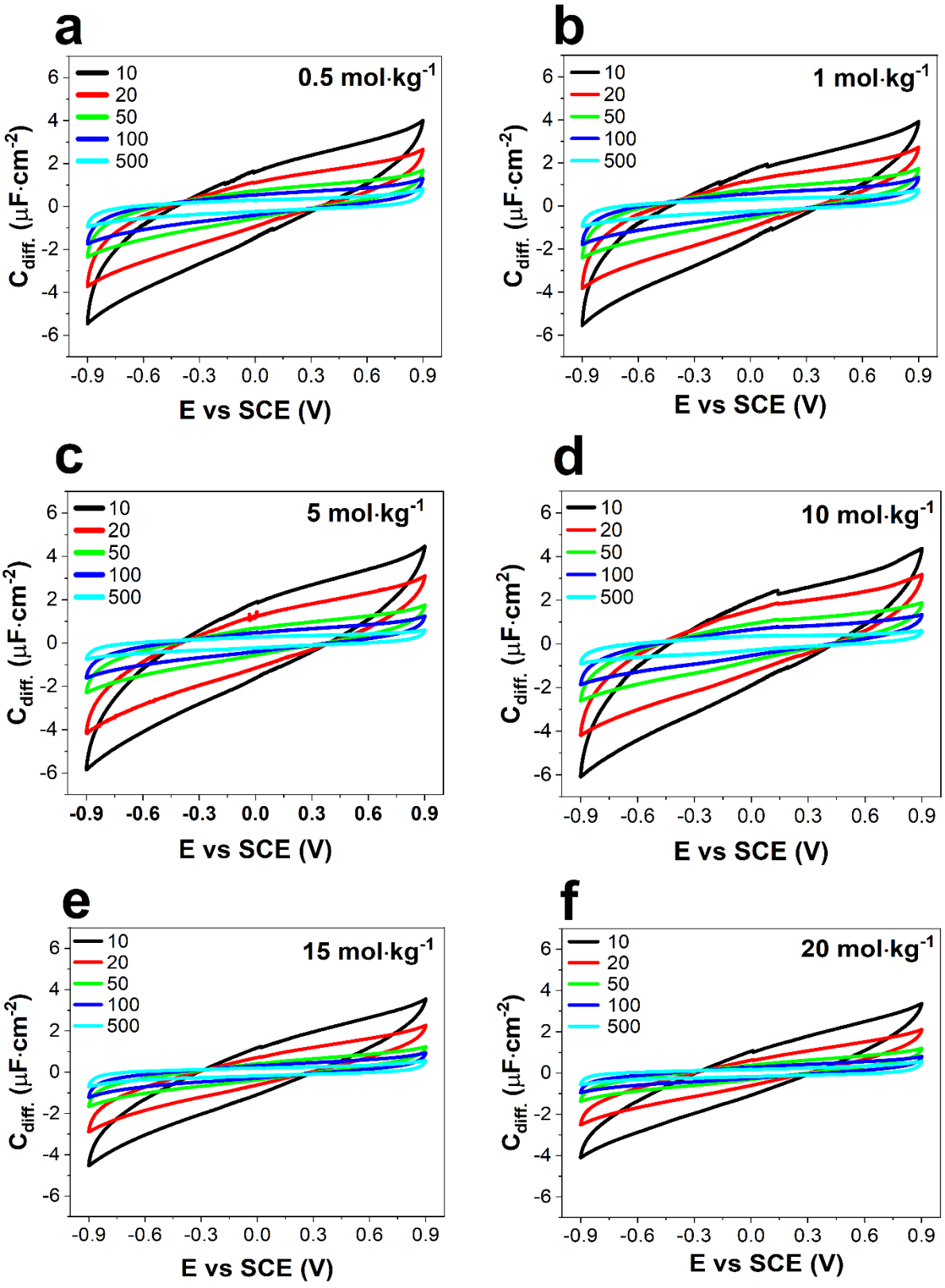

***Figure S8*:** Differential capacitance (normalized current density with scan rate) measured with a non-porous glassy carbon electrode in different LiTFSI solutions (**a-f**) using a three-electrode glass cell at 25 ℃ and scan rates of 10, 20, 50, 100 and 500 $mV \cdot s^{-1}$.

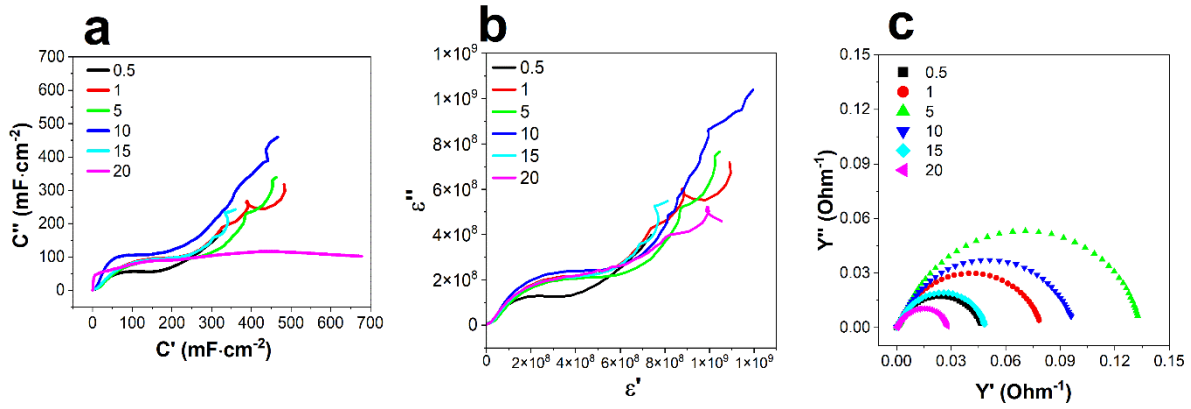

***Figure S9*:** Effect of LiTFSI concentration on the **(a)** Cole-Cole capacitance plot; **(b)** Cole-Cole permittivity plot; and **(c)** Nyquist admittance plot measured with a non-porous stainless-steel electrode

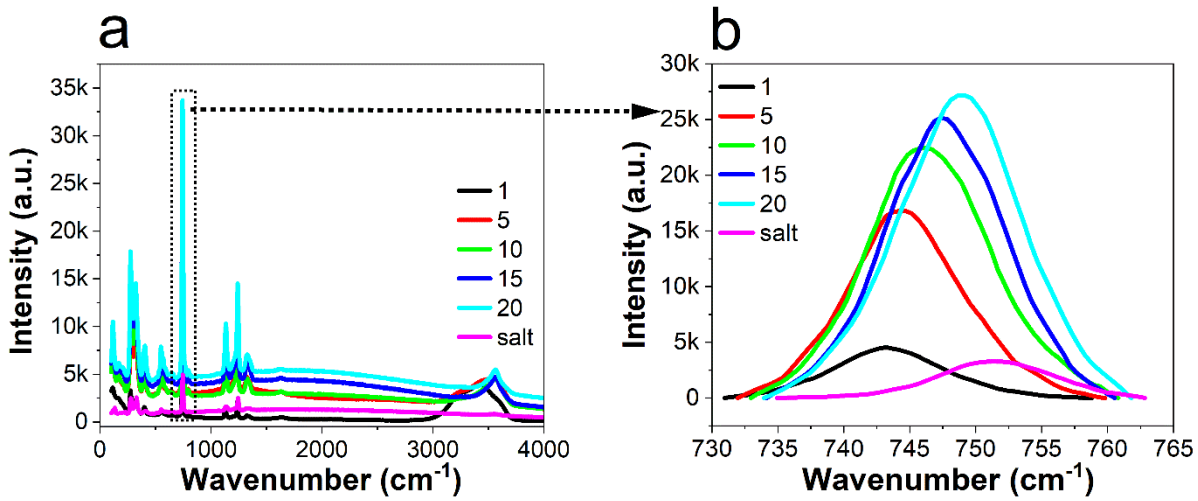

Figure S10: Raman spectra of **(a)** different concentrations of water-in-LiTFSI and solid crystalline salt from 4000 to 120 cm^{-1}; and **(b)** magnified sulfur-nitrogen-sulfur band from 730 to 765 cm^{-1} used for the analysis of ion-pairing.

***Table S1*:** Intensity (I), position (P), width (W), and area (A) of several Raman bands at 740 cm^{-1} (free anion) and 744 cm^{-1} (loose ion pair) for different concentrations of LiTFSI obtained by deconvolution fitting.

Conc. (mol·kg^{-1})	**740 (1_FA)**				**744 (2_LIP)**				**Chi-square**	**R-square**
	I /a.u. (k)	**P /cm^{-1}**	**W /cm^{-1}**	**A /a.u.**	**I /a.u. (k)**	**P /cm^{-1}**	**W /cm^{-1}**	**A /a.u.**		
1	1.27	738 ±2	7.97 ±1.7	10888 ±7867	3.07	743.47 ±0.3	6.82 ±0.93	22345 ±18442	0.9996	0.9995
10	No peak				12.2	744.12 ±0.6	9.48 ±1.06	116582 ±94125	0.9983	0.9985
20					1.61	743.94± 1.1	5.94± 4.64	8713 ±2724	0.9989	0.9989

***Table S2*:** Intensity (I), position (P), width (W), and area (A) of several Raman bands at 746.5 cm^{-1} (intimate ion pair), and 748 cm^{-1} (aggregate ion pair) for different concentrations of LiTFSI obtained by deconvolution fitting.

Conc. (mol·kg^{-1})	**746.5 (3_IIP)**				**748 (4_AGP)**				**Chi-square**	**R-square**
	I /a.u. (k)	**P /cm^{-1}**	**W /cm^{-1}**	**A /a.u.**	**I /a.u. (k)**	**P /cm^{-1}**	**W /cm^{-1}**	**A /a.u.**		
1	1.56	747.31 ±2.6	9.34 ±2.2	15593 ±12000	No peak				0.9996	0.9995
10	11.69	747.55±1.2	9.48± 1.06	138085 ±94399					0.9983	0.9985
20	6.73	747.26±2.0	13.19 ±5.94	92166 ±17723	20.6	749.19 ±1.14	10.32 ±8.3	223235 ±18075	0.9989	0.9989

***Table S3*:** Fractions the ion pairs found in this study and those reported by Suo et al.[3]

Conc. (mol·kg^{-1})	% of ion-pair found in this work				% of ion-pair found by Suo et al.[3]			
	FA	LIP	IIP	AGP	FA	LIP	IIP	AGP
1	22.3	45.8	31.9	0	26.8	45.2	28.0	0
10	0	45.8	54.2	0	0	48.8	52.2	0
20	0	2.7	28.4	68.9	0	7.0	11.0	82.0

***Table S4*:** Diffusivity of Li^+ in m^2s^{-1} from relevant PFG-NMR studies of bulk solutions.[1]

Conc. ($mol \cdot kg^{-1}$)	Z. Li *et al.*[4]	Borodin *et al.*[5]	Han *et al.*[6]	Abbas *et al.*[7]	Average	Standard deviation
1		9E-10	8.70E-10	7.00E-10	8.23E-10	8.80E-11
5		6.3E-10	6.10E-10	3.70E-10	5.36E-10	1.18E-10
10		2.6E-10	2.40E-10	2.00E-10	2.33E-10	2.49E-11
15	1.3E-10	1.3E-10		1.00E-10	1.2E-10	1.41E-11
20	5.6E-11	7.5E-11	6.00E-11	6.00E-11	6.28E-11	7.25E-12

***Table S5*:** Diffusivity of $TFSI^-$ in m^2s^{-1} from relevant PFG-NMR studies of bulk solutions.[1]

Conc. ($mol \cdot kg^{-1}$)	Z. Li *et al.*[4]	Borodin *et al.*[5]	Han *et al.*[6]	Abbas *et al.*[7]	Average	Standard deviation
1		6.90E-10	6.30E-10	5.50E-10	6.23E-10	5.73E-11
5		3.00E-10	2.90E-10	2.50E-10	2.8E-10	2.16E-11
10		9.00E-11	8.50E-11	9.50E-11	9E-11	4.08E-12
15	6.5E-11	7.00E-11		4.50E-11	6E-11	1.08E-11
20	2.4E-11	2.50E-11	2.00E-11	2.50E-11	2.35E-11	2.06E-12

Method S5: Determination of ion-pair (mutual) diffusivity from self-ion diffusivity.[8]

According to the Nernst-Einstein equation, the diffusivity of ion-pairs D_σ using the experimental molar ionic conductivity Λ_{EIS} can be derived from **equation S12**

$$D_\sigma = \frac{N_A \cdot e^2}{k_B \cdot T} \cdot \Lambda_{\mathrm{EIS}} \qquad \textbf{S12}$$

Here, N_A is Avogadro's number ($6.023\times10^{23}\ mol^{-1}$), e is the elementary charge (1.602×10^{-19} C), In addition, effective ionic diffusivities can be calculated from the PFG-NMR based self-ion diffusivity using **equations S13** and **S14**

$$D_+^{eff} = \frac{1}{2}(D_\sigma + D_+^{NMR} - D_-^{NMR}) \qquad \textbf{S13}$$

$$D_-^{eff} = \frac{1}{2}(D_\sigma + D_-^{NMR} - D_+^{NMR}) \qquad \textbf{S14}$$

As such we not only just separated the charged species from the neutral aggregates, but also eliminated part of the ionic diffusivities associated with interaction (friction) between ions whatsoever, also for cases in which they do not form complexes with each other. In this regard, D_+^{eff} and D_-^{eff} would represent binary diffusivities required for the implementation of the concentrated solution theory based on the Onsager-Stefan-Maxwell formalism with **equation S15.**[8]

$$D_{+-} = \frac{1}{2}\,(D_+^{eff} + D_-^{eff}) \qquad \textbf{S15}$$

***Table S6*:** Average diffusivity of LiTFSI, ionic tortuosity of LiTFSI, diffusivity of H_2O[4], and ionic tortuosity of H_2O with standard deviation.[1]

Conc. (mol·kg^{-1})	σ (mS·cm^{-1})	D_{LiTFSI} from σ (m^2s^{-1})	D_{LiTFSI} (m^2s^{-1})		Ionic tortuosity LiTFSI					D_{H2O} (m^2s^{-1})[4]	Ionic tortuosity H_2O
			Average	SD	Min	Mid	max	Average	SD		
1	30.84	8.226E-10	4.11E-10	7.27E-11	1.00	1.00	1.00	1.00		1.01E-09	1.00
5	49.27	2.628E-10	1.31E-10	6.99E-11	2.41	3.13	5.501	3.68	1.62	8.00E-10	1.26
10	35.93	9.582E-11	4.79E-11	1.45E-11	7.75	8.59	10.139	8.83	2.21	2.70E-10	3.74
15	17.45	3.103E-11	1.55E-11	1.25E-11	17.30	26.51	111.27	51.69	30.15	1.20E-10	8.42
20	10.65	1.420E-11	7.10E-12	4.66E-12	41.16	57.95	138.87	79.33	52.24	1.01E-10	10.0

***Table S7*:** Experimental ionic conductivity σ, dynamic viscosity η, molar ionic conductivity Λ_{EIS}, calculated molar ionic conductivity using Nernst-Einstein equation (Λ_{NE}) [9], average ionicity values calculated from the ratio of Λ_{EIS} to Λ_{NE} in this study and the study of Abbas et al.[1,7]

Concentration (mol·kg^{-1})	σ (mS·cm^{-1})	η (mPa·s)	LiTFSI		Ionicity	
			Λ_{EIS} (mS·cm^2·mol^{-1})	Λ_{NE} (mS·cm^2·mol^{-1})	Average	SD
1	30.84	1.57	30.84	54.24	0.64	0.03
5	49.27	4.92	9.85	30.62	0.35	0.025
10	35.93	9.68	3.59	12.12	0.29	0.03
15	17.45	26.22	1.16	6.75	0.17	0.027
20	10.65	53.49	0.53	3.23	0.11	0.045

Method S6: Determination of effective hydrodynamic radii (R_H)[1]

To obtain R_H values of LiTFSI solutions, two steps were followed. Firstly, the Stokes radii of Li^+ (**Table S8**) and $TFSI^-$ (**Table S9**) were calculated using the Stokes-Einstein equation from the diffusivity mentioned in **Tables S4** and **S5**.[4–7] Subsequently, those Stokes radii of Li^+ and $TFSI^-$ were corrected using the calibration curve proposed by Nightingale to derive R_H values.[10] The hydrodynamic radii are often calculated inappropriately small from Stokes's law, because water is not a continuous medium and the radii of the hydrated ions usually are not sufficiently large compared to that of a water molecule for the conditions of viscous flow to be fulfilled.[10] The sum of R_H of Li^+ and $TFSI^-$ can be regarded as the R_H of LiTFSI as listed in **Table S10**. Likewise, the diffusivity of H_2O in various electrolyte concentrations were used for deriving R_H.[4]

***Table S8*:** Stokes radii of Li^+ in m from relevant PFG-NMR studies using the Stokes-Einstein equation.

Conc. ($mol \cdot kg^{-1}$)	Z. Li et al.[4]	Borodin *et al.*[5]	Han *et al.*[6]	Abbas *et al.*[7]	Average	Standard deviation
1	Not available	1.54E-10	1.60E-10	1.99E-10	1.71E-10	1.97E-11
5	Not available	7.04E-11	7.27E-11	1.20E-10	8.76E-11	2.28E-11
10	Not available	8.67E-11	9.39E-11	1.13E-10	9.78E-11	1.10E-11
15	6.85E-11	6.40E-11	Not available	8.32E-11	7.19E-11	8.20E-12
20	7.64E-12	5.44E-11	6.80E-11	6.80E-11	4.95E-11	2.48E-11

***Table S9*:** Stokes radii of TFSI- in m from relevant PFG-NMR studies using the Stokes-Einstein equation.

Conc. ($mol \cdot kg^{-1}$)	Z. Li et al.[4]	Borodin *et al.*[5]	Han *et al.*[6]	Abbas *et al.*[7]	Average	Standard deviation
1	Not available	2.01E-10	2.21E-10	2.53E-10	2.25E-10	2.11E-11
5	Not available	1.48E-10	1.53E-10	1.77E-10	1.59E-10	1.29E-11
10	Not available	2.50E-10	2.65E-10	2.37E-10	2.51E-10	1.14E-11
15	1.37E-10	1.19E-10	Not available	1.85E-10	1.47E-10	2.79E-11
20	1.78E-11	1.63E-10	2.04E-10	1.63E-10	1.37E-10	7.08E-11

***Table S10*:** Effective hydrodynamic radii (R_H) in m of Li^+, $TFSI^-$, LiTFSI, and H_2O.[1]

Conc. ($mol \cdot kg^{-1}$)	Li^+	SD Li^+	$TFSI^-$	SD $TFSI^-$	LiTFSI	SD LiTFSI	H_2O
1	3.50E-10	1.97E-11	3.72E-10	2.11E-11	7.22E-10	4.08E-11	3.3E-10
5	3.10E-10	2.28E-11	3.59E-10	1.29E-11	6.69E-10	3.57E-11	3.01E-10
10	3.18E-10	1.10E-11	3.85E-10	1.14E-11	7.03E-10	2.24E-11	3.15E-10
15	3.05E-10	8.20E-12	3.35E-10	2.79E-11	6.40E-10	3.61E-11	3.08E-10
20	2.70E-10	2.48E-11	3.27E-10	7.08E-11	5.97E-10	8.28E-11	2.91E-10

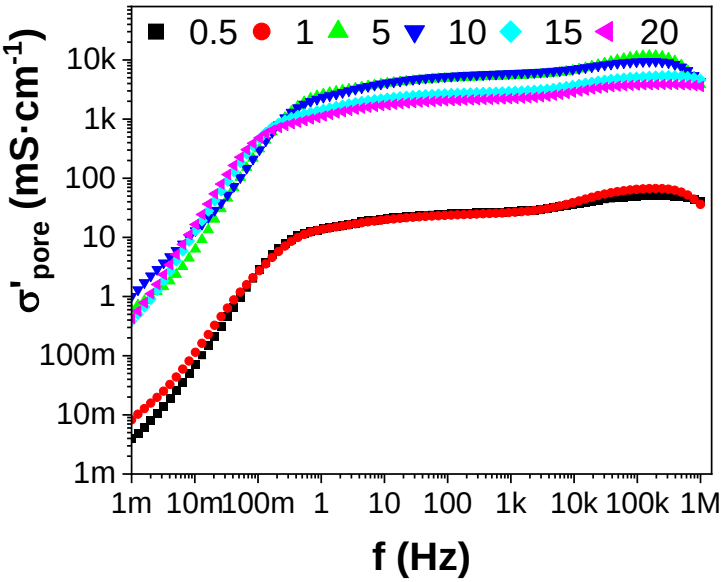

***Figure S11*:** Real part of conductivity vs frequency of electrochemical capacitor cells assembled with porous carbon electrodes for different LiTFSI concentrations (mol·kg^{-1}) operated at open circuit potential.

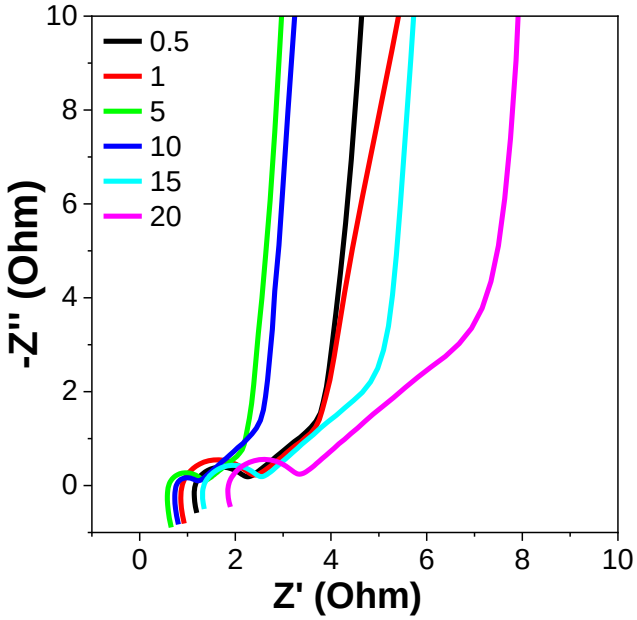

***Figure S12*:** Nyquist impedance plot of electrochemical capacitor cells assembled with porous carbon electrode in different LiTFSI concentrations (mol·kg^{-1}) at open circuit potential ≈30 mV.

Method S7: Determination of MacMullin number of the porous carbon electrode[1]

The ionic resistance in pores $R_{\text{in-pore}}$ was calculated from C'' and f obtained from **Figure 4c** using **equation S16**

$$R_{\text{in-pore}} = \frac{1}{f \cdot C_{EDL,max}} \qquad \textit{(S16)}$$

Here, $C_{\text{EDL, max}}$ is the maximum EDL capacitance after normalization to the geometric area of the carbon sheet.

The $R_{\text{in-pore}}$ value was then used to calculate the effective ionic tortuosity $\mho$ with a modification of the combined MacMullin number and Ohm's law (**equation S17**).[11]

$$\mho = \frac{R_{ion} \cdot A \cdot \sigma}{2d} \cdot CSA\% \qquad \textit{(S17)}$$

Here, A is the geometrical area of the porous carbon electrode, σ is the ionic conductivity of the bulk electrolyte, and d is the thickness of the carbon sheet placed in each electrode of the cell. The cumulative surface area percentage (CSA%) was determined from a N_2 gas adsorption analysis (**Figure S13**). The effective ion diffusivity within the carbon nanopore was calculated with the relationship proposed by MacMullin et al. **(equation S18)** [12,13].

$$D_{\text{eff}} = D_{\text{bulk}} \cdot \frac{\emptyset}{\mho} = \frac{D_{bulk}}{N_M} \qquad \textit{(S18)}$$

Here, D_{eff} is the effective in-pore diffusion coefficient of the ions, D_{bulk} is the diffusion coefficient of the ions in the bulk electrolyte, and $\emptyset$ is the porosity of the carbon electrode. The ionic conductivity σ of the bulk electrolytes was determined by EIS (**Table S7**).

Pore configurations of the carbon electrode (YP80 F), were determined from N_2 gas adsorption and desorption isotherms (**Figure S13**). The specific surface area and the pore size distribution of the carbon were estimated and presented in **Table S11** by applying the QS-DFT adsorption model for slit, cylindrical-shaped pores.[14]

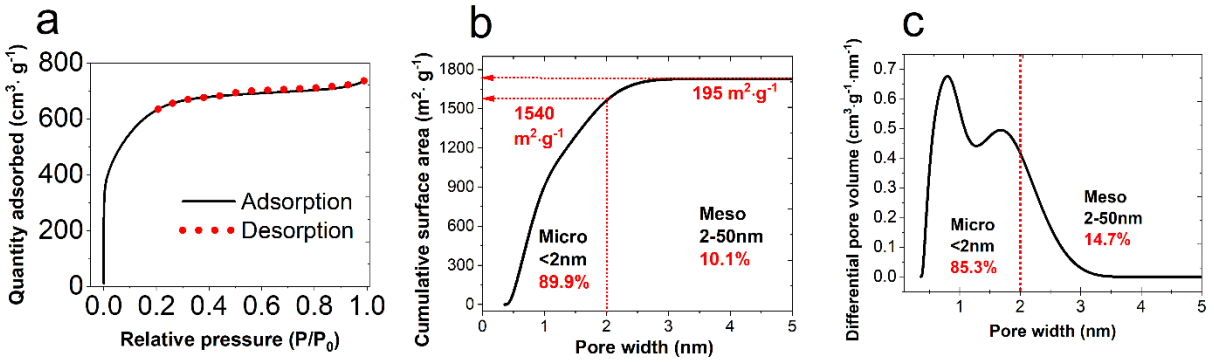

***Figure S13*: a)** Nitrogen gas adsorption and desorption isotherm at a temperature of 77 K, **b)** cumulative surface area, and **c)** differential pore volume and of YP80F carbon electrode which is utilized to assemble the electrochemical capacitor cells.

***Table S11*:** Pore configuration of YP80F from N_2 gas adsorption.

Feature	**Values**
Total cumulative surface area	1735 $m^2 \cdot g^{-1}$
Total BET surface area	2307 $m^2 \cdot g^{-1}$
Volume of the micropores (< 2 nm)	0.80 $cm^3 \cdot g^{-1}$
Volume of the mesopores (2-50 nm)	0.23 $cm^3 \cdot g^{-1}$
Volume fraction of micropores	85.3 %
Volume fraction mesopores	14.7 %
Surface area fraction micropore	89.9 %
Surface area fraction mesopore	10.1 %

Measurements of two-electrode symmetric cells cannot distinguish the electrochemical behavior of the positive and negative electrode. Hence, the modified Darken's relationship of binary diffusivity was utilized as proposed by Krachkovskiy et al. for obtaining bulk ion-pair (mutual) diffusivity values D_{LiTFSI} from their self-ion diffusivity as detailed in **Method S5**.[8]

The effect of pore confinement was considered for extracting R_{micro}, R_{meso}, C''_{micro}, and C''_{meso} from D_{micro} and D_{meso} using **equations S19** to **S24** by merging **equations S16- S18**. To do so, the T' values were determined with **equations S19** and **12**, respectively.[1]

$$\mho'_{micro} = \frac{R_{in-pore} \cdot A \cdot \sigma}{2d} \cdot (1 - CSA\%_{micro}) \quad \textbf{(S19)}$$

$$\mho'_{meso} = \frac{R_{in-pore} \cdot A \cdot \sigma}{2d} \cdot (1 - CSA\%_{meso}) \quad \textbf{(S20)}$$

$$R_{micro} = \frac{2 \cdot d \cdot \mho'_{micro}}{A \cdot \sigma \cdot \emptyset_{micro}} \quad \textbf{(S21)}$$

$$R_{meso} = \frac{2 \cdot d \cdot \mho'_{meso}}{A \cdot \sigma \cdot \emptyset_{meso}} \quad \textbf{(S22)}$$

$$C''_{micro} = \frac{1}{R_{micro} \cdot f} \quad \textbf{(S23)}$$

$$C''_{meso} = \frac{1}{R_{meso} \cdot f} \quad \textbf{(S24)}$$

Here, $\mho'_{\mathrm{micro}}$ and $\mho'_{\mathrm{meso}}$ is the tortuosity considering micro and mesopore confinement effects, respectively.

***Table S12*:** Effect of LiTFSI concentration on effective in-pore diffusivity of LiTFSI, tortuosity, $R_{in\text{-}pore}$, C''_{max} within the micro- and mesopores.[1]

LiTFSI conc. (mol·kg^{-1})	D_{bulk} (10^{-11} ·m^2·s^{-1})	Effective $D_{in\text{-}pore}$ (10^{-11} · m^2·s^{-1})		Effective tortuosity		$R_{in\text{-}pore}$ (Ohm·cm^2)			C''_{max} (F·g^{-1})		
		Micro	Meso	Micro	Meso	Micro	Meso	Total from EIS	Micro	Meso	Total from EIS
1	41.13	1.48	13.37	23.70	0.46	3.56	31.69	35.25	89.65	10.07	9.05
5	13.14	0.41	3.66	27.72	0.54	2.46	21.90	24.36	107.2	12.04	10.83
10	4.79	0.21	1.91	19.54	0.38	2.39	21.30	23.69	97.17	10.92	9.81
15	1.55	0.07	0.59	20.30	0.39	4.95	44.06	49.01	106.0	11.96	10.81
20	0.71	0.04	0.33	14.20	0.27	6.00	53.42	59.41	114.8	12.90	11.60

Table S13: Details of $C_{EDL,\ in\text{-}pore}$ calculation from the characteristic frequency at maximum imaginary conductivity plot (**Figure 4e**) using **equation 1**.

Salt conc. (mol·kg^{-1})	f_0 from max. σ'' in pore (Hz)	R_s (Ohm)	Time constant (μs)	C_{EDL} (μF/cm^2)	C_{EDL} (μF/g)
0.5	15124.000	1.250	10.523	10.719	1054.572
1	19095.200	0.951	8.335	11.159	1074.840
5	24096.300	0.670	6.605	12.552	1197.100
10	19095.200	0.809	8.335	13.111	1149.907
15	15124.000	1.370	10.523	9.780	835.100
20	11987.800	1.897	13.276	8.913	777.788

***Table S14*:** Ion-pair radii or size i.e. R_H (nm) in LiTFSI with corresponding cumulative surface area (CSA) at similar pore width similar to radii of cation-cation, anion-anion, cation-anion, and CSA% as a function of salt concentration.

Ion pair type	Salt conc. (mol/kg)	Radii of ion pairs (nm)	Total CSA (m^2/g)	CSA for pore width similar to ion pair radii (m^2/g)	CSA%
Cation-cation in LiTFSI	1	0.701	1735.46	449.97	25.93
	5	0.623		298.09	17.18
	10	0.636		329.97	19.01
	15	0.612		278.24	16.03
	20	0.543		160.12	9.23
Anion-anion in LiTFSI	1	0.744		531.54	30.63
	5	0.718		479.02	27.60
	10	0.772		573.56	33.05
	15	0.671		390.52	22.50
	20	0.654		361.28	20.82
Cation-anion in LiTFSI	1	0.722		489.02	28.18
	5	0.669		389.52	22.45
	10	0.703		449.97	25.93
	15	0.641		334.77	19.29
	20	0.597		261.24	15.05

***Method S8**:* Calculation of the molecular volume of H_2O[1]

Molar mass of water = 0.018 $kg \cdot mol^{-1}$.
∴Number of molecules in 0.018 kg of water: $6 \cdot 10^{23}$ (Avogadro's number)
∴Mass of one molecule of water = $\frac{0.018}{6 \cdot 10^{23}}$ kg = $3 \cdot 10^{-26}$ kg
∴Volume of a water molecule = $\frac{Mass}{Density} = \frac{3 \cdot 10^{-26}}{1000}$ m^3 = $3 \cdot 10^{-29}$ m^3

***Table S15*:** Hydration number of Li^+, $TFSI^-$, LiTFSI ions using their effective hydrodynamic radii (R_H) in bulk electrolytes

LiTFSI conc. ($mol \cdot kg^{-1}$)	Bulk solution		
	Li^+	$TFSI^-$	LiTFSI
1	5.94	2.35	8.29±0.712
5	4.12	1.62	5.74±0.249
10	4.45	3.13	7.58±0.371
15	3.92	0.41	4.33±0.207
20	2.71	0.04	2.76±0.314

Method S9: Determination of diffuse layer length and time-constant in porous carbon from the loss tangent of electrochemical capacitor cells

The diffuse layer length for several concentrations of water-in-salt electrolytes were determined utilizing the maximum dielectric loss tangent (*tan δ*) determined from the ratio of ε'' over ε' using equations **S25** and **S26**.[15] ε', ε'', and *tan δ* are shown in **Figures S12a**, **S12b** and **S12c**, respectively. The diffusion time constant was calculated using the frequency position of the maximum *tan δ* from **equation S27**.

$$tan\,\delta = \frac{\varepsilon''}{\varepsilon'} \qquad \textbf{(S25)}$$

$$Diffuse\ layer\ length = \frac{d}{(2\ tan\ \delta_{max})^2} \qquad \textbf{(S26)}$$

$$Time\ constant\ from\ loss\text{-}tangent = \frac{1}{2\cdot\pi\cdot f_{tan\,\delta\,max}} \qquad \textbf{(S27)}$$

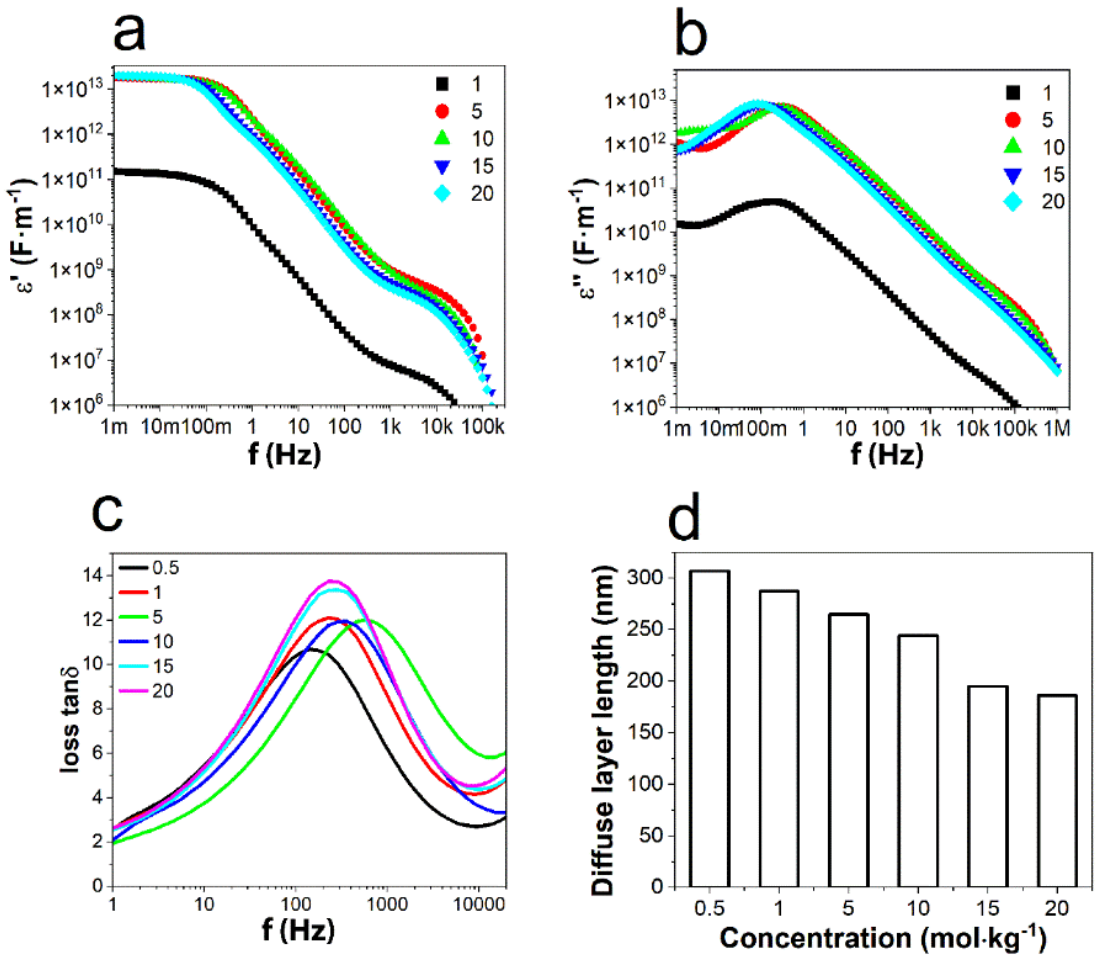

Figure S14**:** Concentration-dependent permittivity **a)** real part, **b)** imaginary part, **c)** loss tangent plot, and **d)** diffuse layer length of porous carbon electrode in electrochemical capacitor cell with LiTFSI electrolyte operated at open circuit potential.

***Method S10*:** Determination of energy density of electrochemical capacitor cells

The energy density was calculated from the impedance spectra recorded at 0.4, 0.8 and 1.2 V using equations **S28** and **S29**.[16]

$$E=\frac{C_{S*A*\Delta V^2}}{2m*3.6} \qquad \textit{(S288)}$$

$$Cs=\frac{1}{2\pi f\cdot Z''} \qquad \textit{(S29)}$$

Here, *Cs* is the series capacitance, *A* is the geometrical area of the carbon electrode, ΔV is the applied potential, *m* is the total mass of both electrodes, *f* is the frequency, *Z''* is the imaginary component of the impedance. The Nyquist plot, series capacitance and energy density for all concentrations of LiTFSI at different voltages are shown in **Figure S15**.

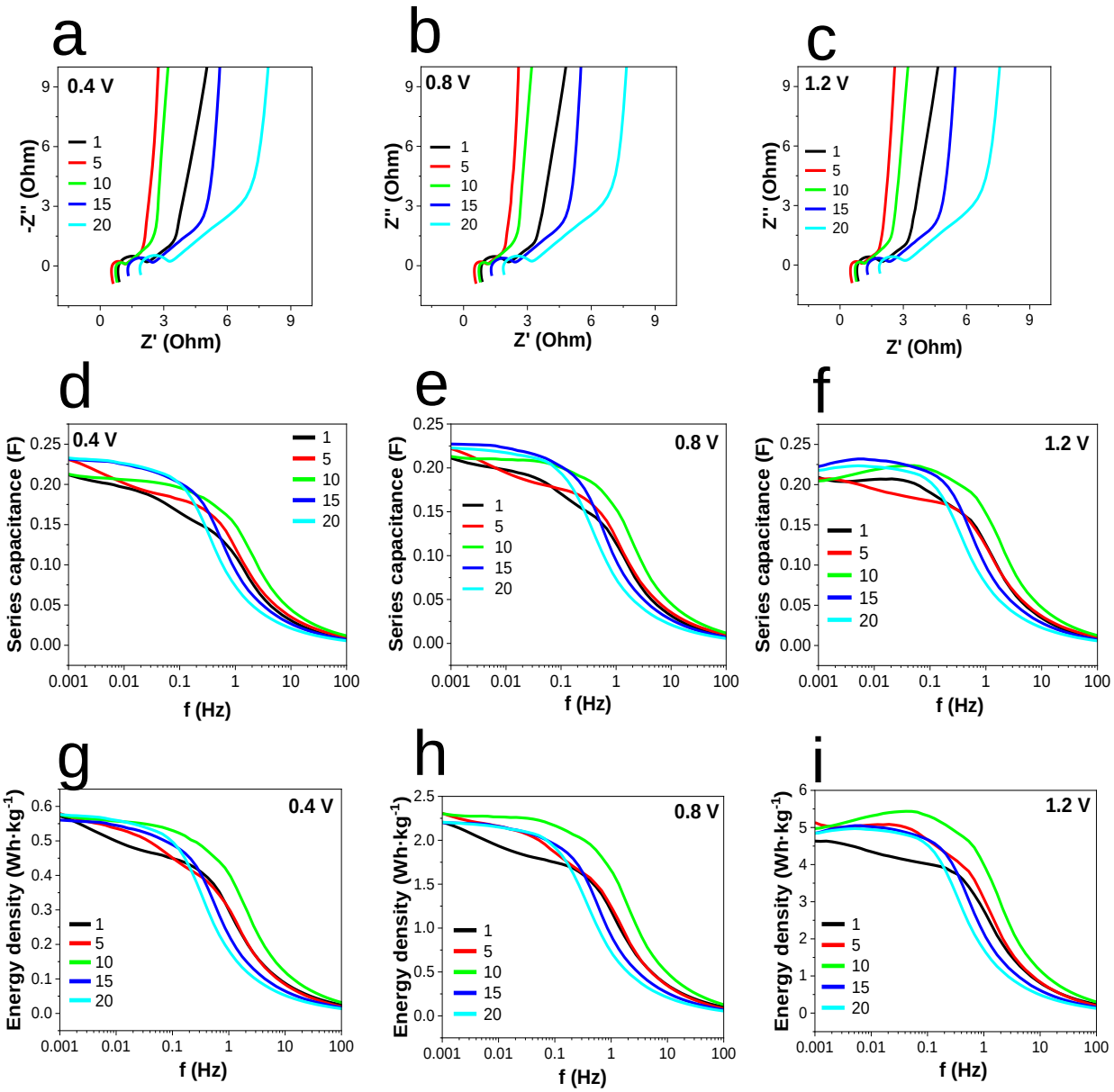

Figure S15: Effect of LiTFSI concentration and voltage on the Nyquist plot (**a-c**), series capacitance (**d-f**) and energy density (**g-i**) of capacitor cells.

Method S11: Power determination of electrochemical capacitor cells

Active power (P') and reactive power (P'') were calculated using **equations S28** and **S29** and shown in **Figures S13a** and **S13b**, to characterize the capacitor cells from the electrical point of view.[16]

$$P' = C'' * |\Delta V_{rms}|^2 \quad \textbf{(S28)}$$

$$P'' = -C' * |\Delta V_{rms}|^2 \quad \textbf{(S29)}$$

$|\Delta V_{rms}|^2 = \Delta V_{max}/\sqrt{2}$, where V_{max} is the maximum amplitude of the AC voltage (5 mV).[16] We directly obtained the $|\Delta V_{rms}|$ values from the EC-lab software as a function of frequency.

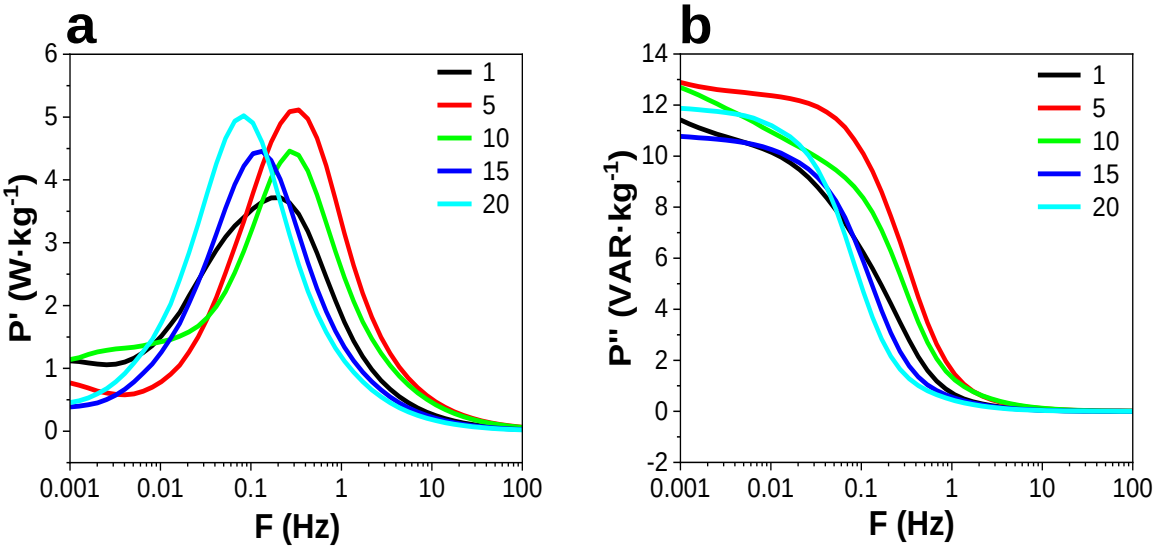

Figure S16**:** Concentration-dependent power density electrochemical capacitor cells assembled with LiTFSI, operating at open circuit potential **a)** active power and **b)** reactive power.

Table S16: Time constants ($1/2 \cdot \pi \cdot f$) obtained from the frequency position of maximum imaginary conductivity, maximum imaginary capacitance, maximum active power density, and tan δ.

Salt conc. (mol·kg^{-1})	Time constant from f of σ''_{bulk} max. (μs)	Time constant from f of σ''_{pore} max. (µs)	Time constant from f of c'' max. (ms)	Time constant from f of P′ max. (ms)	Time constant from f of tan δ max. (µs)
0.5	65.34	10.52			663.14
1	47.95	8.33	527.4	875.92	1009.22
5	41.09	6.61	440.1	499.39	446.94
10	35.18	8.34	421.9	600.13	271.32
15	65.35	10.52	987.3	1209.38	618.56
20	103.99	13.28	1256	1242.42	683.21

References

(1) Islam, M. T.; Gollas, B.; Abbas, Q. Differentiating Ion Transport of Water-in-Salt Electrolytes within Micro- and Meso-Pores of a Multiporous Carbon Electrode. *J Mater Chem A Mater* **2024**. https://doi.org/10.1039/d4ta03632h.

(2) Orazem, M. E.; Tribollet, B. *Electrochemical Impedance Spectroscopy*; John Wiley & Sons, Inc: Hoboken, NJ, 2008. https://doi.org/10.1002/9780470381588.

(3) Suo, L.; Oh, D.; Lin, Y.; Zhuo, Z.; Borodin, O.; Gao, T.; Wang, F.; Kushima, A.; Wang, Z.; Kim, H. C.; Qi, Y.; Yang, W.; Pan, F.; Li, J.; Xu, K.; Wang, C. How Solid-Electrolyte Interphase Forms in Aqueous Electrolytes. *J Am Chem Soc* **2017**, *139* (51), 18670–18680. https://doi.org/10.1021/jacs.7b10688.

(4) Li, Z.; Bouchal, R.; Mendez-Morales, T.; Rollet, A. L.; Rizzi, C.; Le Vot, S.; Favier, F.; Rotenberg, B.; Borodin, O.; Fontaine, O.; Salanne, M. Transport Properties of Li-TFSI Water-in-Salt Electrolytes. *Journal of Physical Chemistry B* **2019**, *123* (49), 10514–10521. https://doi.org/10.1021/acs.jpcb.9b08961.

(5) Borodin, O.; Suo, L.; Gobet, M.; Ren, X.; Wang, F.; Faraone, A.; Peng, J.; Olguin, M.; Schroeder, M.; Ding, M. S.; Gobrogge, E.; Von Wald Cresce, A.; Munoz, S.; Dura, J. A.; Greenbaum, S.; Wang, C.; Xu, K. Liquid Structure with Nano-Heterogeneity Promotes Cationic Transport in Concentrated Electrolytes. *ACS Nano* **2017**, *11* (10), 10462–10471. https://doi.org/10.1021/acsnano.7b05664.

(6) Han, K. S.; Yu, Z.; Wang, H.; Redfern, P. C.; Ma, L.; Cheng, L.; Chen, Y.; Hu, J. Z.; Curtiss, L. A.; Xu, K.; Murugesan, V.; Mueller, K. T. Origin of Unusual Acidity and Li+Diffusivity in a Series of Water-in-Salt Electrolytes. *Journal of Physical Chemistry B* **2020**, *124* (25), 5284–5291. https://doi.org/10.1021/acs.jpcb.0c02483.

(7) Abbas, Q.; Nürnberg, P.; Ricco, R.; Carraro, F.; Gollas, B.; Schönhoff, M. Less Water, Naked Choline, and Solid Iodine for Superior Ecofriendly Hybrid Energy Storage. *Advanced Energy and Sustainability Research* **2021**, *2* (12), 2100115. https://doi.org/10.1002/aesr.202100115.

(8) Krachkovskiy, S.; Dontigny, M.; Rochon, S.; Kim, C.; Trudeau, M. L.; Zaghib, K. Determination of Binary Diffusivities in Concentrated Lithium Battery Electrolytes via NMR and Conductivity Measurements. *Journal of Physical Chemistry C* **2020**, *124* (45), 24624–24630. https://doi.org/10.1021/acs.jpcc.0c07383.

(9) Nordness, O.; Brennecke, J. F. Ion Dissociation in Ionic Liquids and Ionic Liquid Solutions. *Chemical Reviews*. American Chemical Society December 9, 2020, pp 12873–12902. https://doi.org/10.1021/acs.chemrev.0c00373.

(10) Nightingale, E. R. Phenomenological Theory of Ion Solvation. Effective Radii of Hydrated Ions. *Journal of Physical Chemistry* **1959**, *63* (9), 1381–1387. https://doi.org/10.1021/j150579a011.

(11) Landesfeind, J.; Hattendorff, J.; Ehrl, A.; Wall, W. A.; Gasteiger, H. A. Tortuosity Determination of Battery Electrodes and Separators by Impedance Spectroscopy. *J Electrochem Soc* **2016**, *163* (7), A1373–A1387. https://doi.org/10.1149/2.1141607jes.

(12) Macmullin, R. B.; Mucclnl, G. A. Characteristics of Porous Beds and Structures. *AIChE Journal* **1956**, *2* (3), 393-403. https://doi.org/10.1002/aic.690020320.

(13) Xu, J. H.; Schoetz, T.; McManus, J. R.; Subramanian, V. R.; Fields, P. W.; Messinger, R. J. Tunable Pseudocapacitive Intercalation of Chloroaluminate Anions into Graphite Electrodes for Rechargeable Aluminum Batteries. *J Electrochem Soc* **2021**, *168* (6), 060514. https://doi.org/10.1149/1945-7111/ac0648.

(14) Borchardt, L.; Leistenschneider, D.; Haase, J.; Dvoyashkin, M. Revising the Concept of Pore Hierarchy for Ionic Transport in Carbon Materials for Supercapacitors. *Adv Energy Mater* **2018**, *8* (24), 1800892. https://doi.org/10.1002/aenm.201800892.

(15) Nguyen, T. Q.; Breitkopf, C. Determination of Diffusion Coefficients Using Impedance Spectroscopy Data. *J Electrochem Soc* **2018**, *165* (14), E826–E831. https://doi.org/10.1149/2.1151814jes.

(16) Taberna, P. L.; Simon, P.; Fauvarque, J. F. Electrochemical Characteristics and Impedance Spectroscopy Studies of Carbon-Carbon Supercapacitors. *J Electrochem Soc* **2003**, *150* (3), A292. https://doi.org/10.1149/1.1543948.